Laboratory astrophysics in the extreme ultraviolet[1]

J.K. Lepson, P. Beiersdorfer, M. Bitter, and S.M. Kahn

Abstract: Electron beam ion traps are uniquely well suited for laboratory astrophysics because they can produce nearly any charge state of any element in a collisionally excited plasma that is comparable in density and temperature to many astronomical sources. The Lawrence Livermore EBIT facility has been optimized for laboratory astrophysics with a suite of dedicated instruments and has made significant advances in this field. This paper reviews some of the work performed at LLNL in compiling comprehensive spectral catalogues, discovery of a magnetic field line diagnostic in the EUV and soft X-ray regimes, and density diagnostics on EBIT and at the NSTX tokamak.

PACS Nos.: 95.30.Ky, 32.30.Rj, 95.75.−z, 95.85.Nv, 97.10.Ex, 95.55.Ka, 95.85.Mt, 52.55.Fa

Résumé : Les pièges ioniques à faisceau d'électrons sont extrêmement bien adaptés aux recherches en astrophysique dans le laboratoire, parce qu'ils peuvent produire pratiquement n'importe quel état de charge de n'importe quel élément dans des plasmas excités de densités comparables aux densités et températures de plusieurs sources astronomiques. L'appareil EBIT du Lawrence Livermore a été optimisé pour les recherches en astrophysique avec une série d'instruments dédiés et a permis des avances significatives dans ce domaine. Nous passons ici en revue certains travaux exécutés au LLNL , la compilation de catalogues spectraux, la découverte d'un diagnostique de lignes de champ magnétique dans les régimes EUV et X et des diagnostiques de densité sur EBIT et au tokamak NSTX.

[Traduit par la Rédaction]

1. Introduction

X-ray and extreme ultraviolet astronomy has long been hindered by the opacity of Earth's atmosphere in this spectral region. While solar X-rays were first detected in 1949 [1] and extra-solar X-rays in 1962 [2], the development of X-ray and EUV astrophysics was hamstrung by the brevity of infrequent rocket flights. With the launch of satellite-borne detectors, X-ray astrophysics started to take root. Early satellite observatories, such as Uhuru, ROSAT, ASCA, and EUVE, made great strides in the cataloguing of objects and the beginnings of spectroscopy, though the latter was hampered by the low resolving power of the instruments on board. With the advent of high-resolution spectrometers on Chandra and XMM-Newton a decade ago, X-ray astrophysics really began to flourish [3].

Laboratory astrophysics in the X-ray and EUV regions began much later than observations. Although experiments with X-ray emitting plasmas date back to the 1970s, the first experimental facilities dedicated to laboratory astrophysics were built around the EBIT-I and EBIT-II devices at LLNL in the 1990s, and laboratory astrophysics then became a major component of the Livermore group [4–6]. The development of EUV and X-ray laboratory astrophysics at LLNL was spurred by observations undertaken with EUVE in the extreme ultraviolet and ASCA in the X-ray region, which both included puzzling data — unexplained by the contemporary spectral models — and by the then impending deployment of Chandra and XMM-Newton, with the realization that these satellites would return data that were more advanced and more detailed than the available models and databases. Much of the work mentioned here was performed to allow interpretation of high-resolution grating spectrometer spectra from the new generation X-ray satellite observatories in the 20–200 Å wavelength region.

Received 25 June 2007. Accepted 7 August 2007. Published on the NRC Research Press Web site at http://cjp.nrc.ca/ on 5 February 2008.

J.K. Lepson.[2] Space Sciences Laboratory, University of California, Berkeley, CA 94720, USA.
P. Beiersdorfer. Lawrence Livermore National Laboratory Livermore, CA 94550, USA.
M. Bitter. Princeton Plasma Physics Laboratory Princeton, NJ 08543, USA.
S.M. Kahn. Physics Department & SLAC, Stanford University, Stanford, CA 94305, USA.

[1] Paper given at the Workshop on Twenty Years of Spectroscopy with EBIT held in Berkeley, California, 13–15 November 2006.
[2] Corresponding author (e-mail: lepson@ssl.berkeley.edu).

2. X-ray and EUV astrophysics in the laboratory

Collisionally excited X-ray emitting astrophysical plasmas exist at high temperatures (i.e., $5 \times 10^5 - 10^8$ K) and moderate electron densities (i.e., $10^{-3} - 10^{14}$ cm^{-3}). Many laboratory devices produce plasmas (Fig. 1), but most are unsuited for studying X-rays of astrophysical interest because the plasmas they produce are either too cool (for example, glow discharges), too dense (for example, vacuum sparks, z pinches, laser fusion), or both (for example, arcs, theta pinches). Only two laboratory plasma sources, electron beam ion traps and tokamaks (and closely related devices such as stellarators, etc.), provide emission line spectra at the high temperatures and low densities relevant to X-ray astrophysics of collisionally excited plasmas [6]. Electron beam ion traps produce plasmas at lower densities than tokamaks. The spread in densities can be valuable for evaluating density diagnostics when using both devices, as we will show. Electron beam ion traps are especially well suited for laboratory

 doi: 10.1139/P07-167

Fig. 1. Density and temperature regimes of X-ray emitting collisionally excited plasmas.

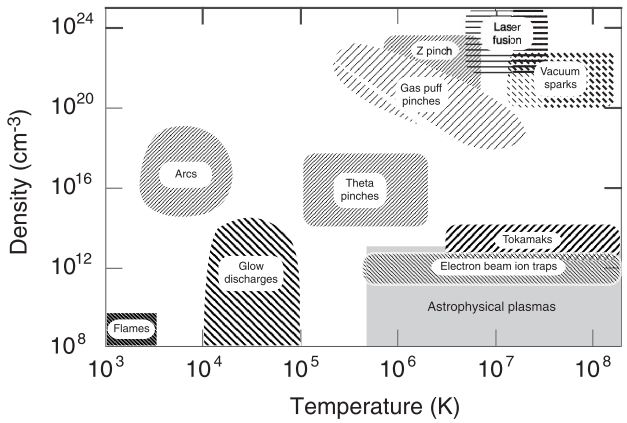

astrophysics because of the ease with which one can produce virtually any charge state of virtually any element [6].

Although it is not the focus of this paper, electron beam ion traps can also mimic conditions found in photoionized plasmas. For example, the charge state of interest can be produced, and the X-rays produced by the recombination effects (both dielectronic and radiative) can be observed by passing a low energy electron beam through the cloud of trapped highly charged ions [7].

The Lawrence Livermore electron beam ion trap facility has been optimized for laboratory astrophysics with a large suite of spectrometers built specifically for astrophysics covering the range from 0.6–400 Å. Spectrometers in use at LLNL include the XRS microcalorimeter (covering 0.2–20 keV), von Hamos type curved crystal spectrometers (1–5 Å), vacuum flat crystal spectrometers (4–25 Å), and grazing incidence spectrometers (10–400 Å) [6].

Most of the work reported on here was performed with the grazing incidence spectrometers. These have a variable line spacing with an average of 1200 lines/mm (for higher wavelengths) or 2400 lines/mm (for lower wavelengths). Data were recorded with liquid nitrogen cooled CCD detectors. Details of the experimental setup may be found in various publications [6, 8].

3. Spectral catalogue

The soft X-ray and extreme ultraviolet spectral region is well known for the richness of its line emission. Many astrophysically important elements have numerous lines in this region, and a number of these lines are useful as diagnostics for temperature and density [9–13].

This region is also well known, however, for the incompleteness of the spectral databases available to astrophysicists. The commonly used databases, such as CHIANTI [14–16] and MEKAL [17], historically included only a fraction of the lines found in the spectra of astrophysical plasmas. As a result, many emission lines, especially the weaker lines, remained unidentified in spectra taken by the Chandra X-ray Observatory and XMM-Newton. Candidates for these lines include mid- to high-charge states of elements such as argon, sulfur, silicon, magnesium, calcium, aluminum, nickel, and iron. The potential for misinterpreting astrophysical spectra because of incomplete databases is well known. A commonly used example is the corona of the nearby star system Alpha Centauri, for which a global fitting model, based on the MEKAL database, of the EUVE spectrum's large apparent continuum, resulted in a differential emission measure distribution with an astrophysically improbable high-temperature tail of $\sim 30 \times 10^6$ K [18]. Laboratory measurements with the LLNL EBIT subsequently found a large number of iron lines that were missing from the models and that form a pseudocontinuum bulge around 60–100 Å (Fig. 2), which affected the results of global fits analyses [19]. Similarly, a fit of the ASCA spectrum of Capella (Alpha Aurigae) could not account for a discrepancy around 10 Å; this was found to be due to Fe XVII emission lines missing from the databases at the time, but which were later observed on EBIT [20]. Other elements also have many lines that were not included in models or databases. An example is argon, which has numerous lines between 20 and 50 Å (Fig. 3), most of which were not in contemporary databases, but many of which have since been added.

We have been actively engaged in a long-term project to compile a comprehensive catalogue of soft X-ray and EUV emission lines for astrophysically important elements (for example, Fe, Ni, Ar, S, Si, Ca, Al, Mg), utilizing the unique high-resolution

Fig. 2. Spectrum of M-shell iron taken on the LLNL electron beam ion trap. Gray fill is a schematic representation of the pseudocontinuum formed by the many weak lines around 60–100 Å. Figure from ref. 6. Reprinted, with permission, from. Ann. Rev. Astron. Astrophy. Vol. 41 (c) 2003 by Annual Reviews. www.annualreviews.org

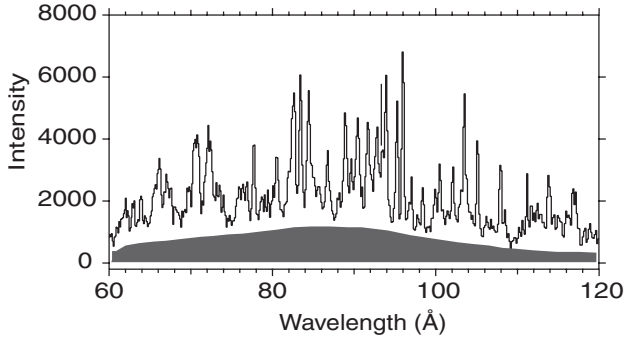

Fig. 3. Spectrum of L-shell argon taken on the LLNL electron beam ion trap showing a pseudocontinuum bulge formed by many weak lines around 30 Å.

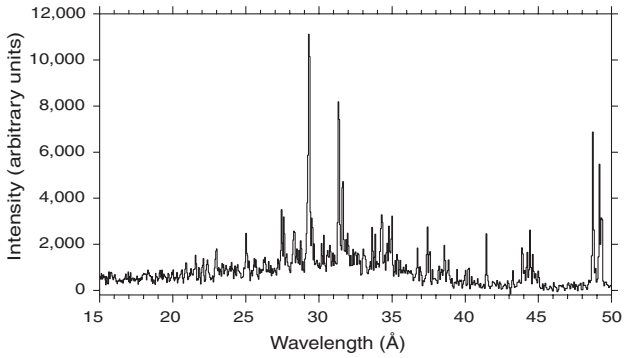

Fig. 4. Comparison of measured and theoretical spectra for Si V – Si VII. The spectrum from EBIT (shaded) was measured at 200 eV beam energy and is overlain with synthetic spectra generated from HULLAC calculations.

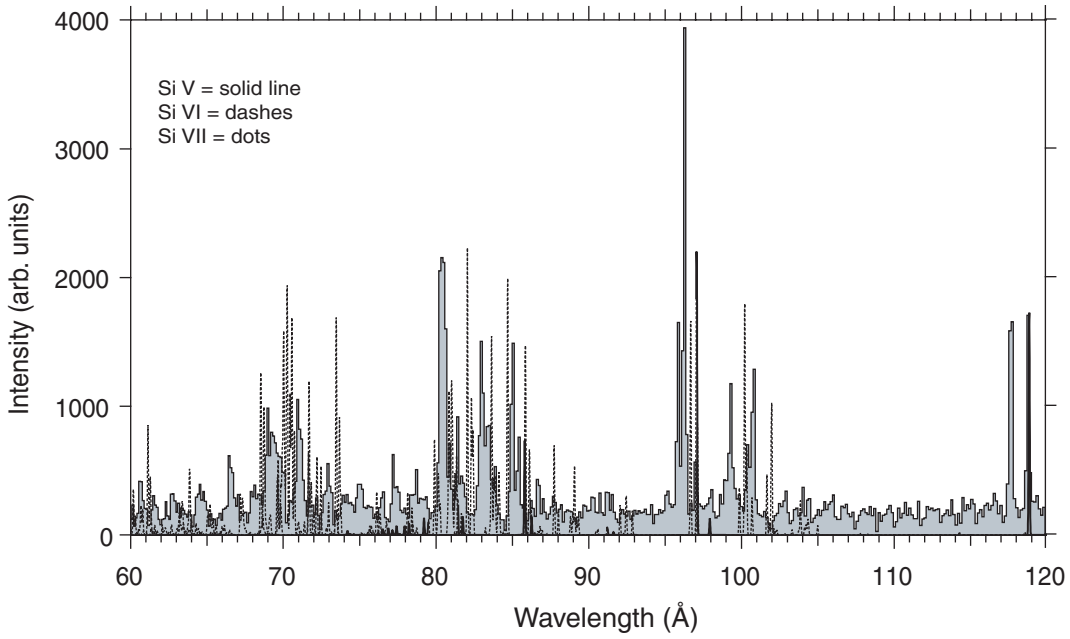

Fig. 5. Comparison of argon spectra taken by broadband high-resolution spectrometer (top) and narrowband ultra high-resolution spectrometer (bottom).

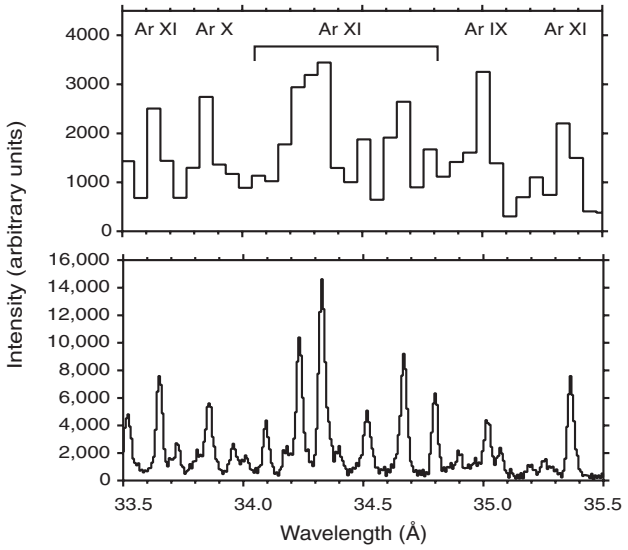

($\sim$ 500 at 50 Å) spectrographic abilities of the LLNL electron beam ion traps in the wavelength region above 20 Å. We have published line lists of M-shell iron (Fe VII–Fe X [21]) and L-shell iron (Fe XVII [20, 22], Fe XVIII – Fe XXIV [23]), nickel (Ni XIX – NiXXVI [24, 25]), argon (Ar IX – Ar XVI [8]), sulfur (S VII – S XIV [26]), and silicon (Si V [27], Si V – Si XII, in preparation). Measurements have also been completed for analyses of magnesium and aluminum. Our line lists include wavelengths, relative strengths, and the emitting atomic transition.

Table 1. Comparison of the number of lines identified in each charge state of L-shell sulfur compared to the line lists in MEKAL and CHIANTI current at time of the EBIT work (2005).

Ion	EBIT	MEKAL	CHIANTI
S VII	10	8	0
S VIII	25	8	0
S IX	22	2	0
S X	29	4	1
S XI	14	1	0
S XII	9	0	4
S XIII	10	0	4
S XIV	8	0	13
TOTAL	135	23	22

Our line lists have significantly contributed to the astrophysical databases. An example is shown in Table 1, which compares our line list for L-shell sulfur with those of CHIANTI [14–16] and MEKAL [17], contemporary with our measurements (2005). We added over 100 lines to the roughly two dozen found in both CHIANTI and MEKAL at that time. Our measurements are now being incorporated into these databases.

Our EUV catalogues are also of value to theory. We used the HULLAC [28, 29] and FAC [30] atomic models to calculate emission from the ions we studied and used those results to construct synthetic spectra, which we used to help identify the lines we measured. However, the complexity of the atomic codes and the difficulties of calculating the many energy levels means that there are some inaccuracies for both line position and intensity. In most cases, the models are accurate enough to readily identify all of the stronger lines for each charge state

Fig. 6. Comparison of Chandra spectrum of Procyon (shaded), adapted from ref. 32 with EBIT spectrum of sulfur (continuous line).

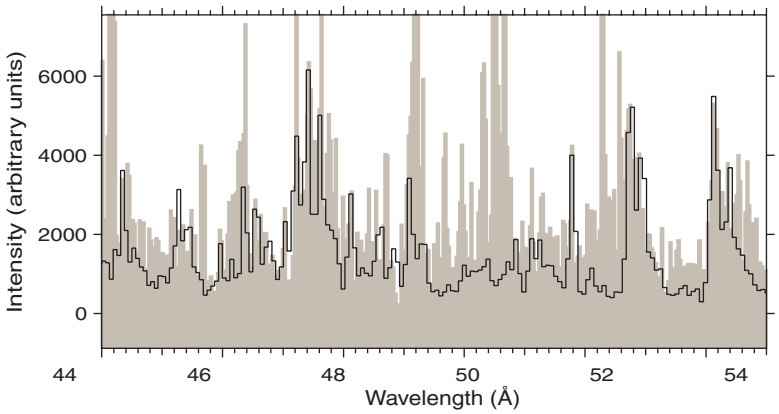

Fig. 7. Density diagnostics for Procyon using the M2/3G line ratio of S VII. Left: EBIT spectrum (continuous line) from ref. 26, Procyon spectrum (shaded) adapted from ref. 32. The broken line outlines larger M2 line observed in Procyon. Right: derivation of the density with the standard deviation of the ratio indicated by broken lines. The ratio curve was calculated with the flexible atomic code [30]. The M2/3G ratio measured in Procyon was 0.7, resulting in a derived log density of 10.5.

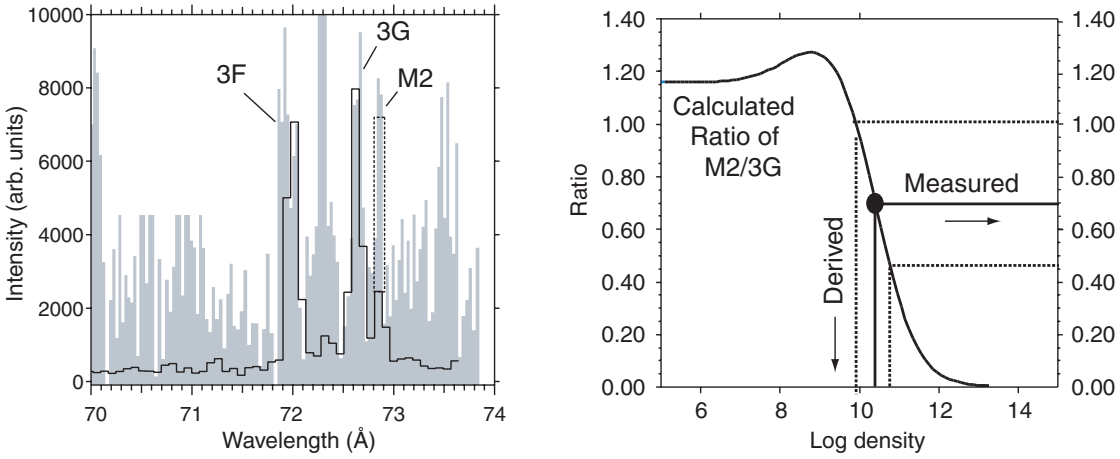

Fig. 8. Magnetic field diagnostic line in argon. Line $\mathcal{B}$ is barely visible at a magnetic field strength of 1 T (left) but is clearly visible at 3 T (right). The figure is from ref. 37.

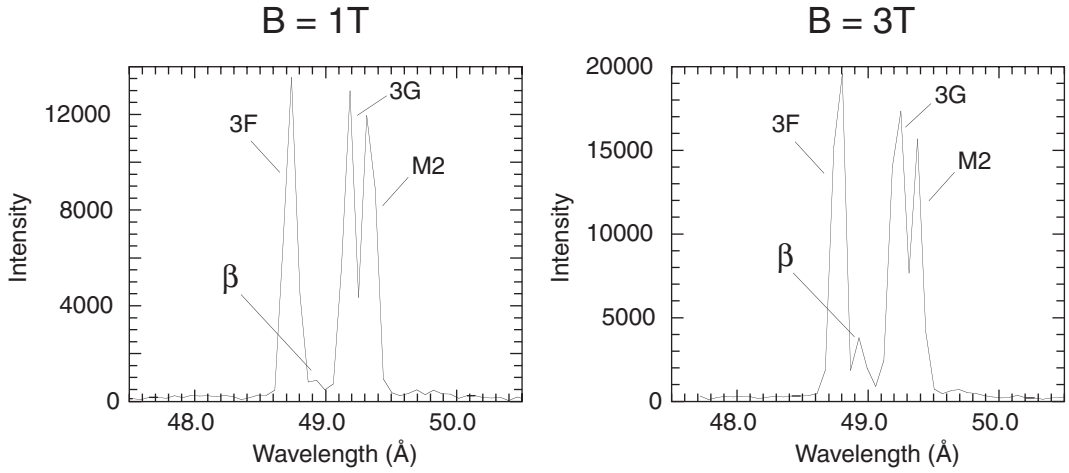

Table 2. Mean deviation of experiment (EBIT) from theory (HULLAC) averaged over all measured lines for neon-like through lithium-like silicon, sulfur, and argon (adapted from ref. 27).

Ion	Δλ	Ion	Δλ	Ion	Δλ
Si V	0.550	S VII	0.257	Ar IX	0.125
Si VI	0.332	S VIII	0.201	Ar X	0.103
Si VII	0.346	S IX	0.214	Ar XI	0.086
Si VIII	0.247	S X	0.171	Ar XII	0.077
Si IX	0.266	S XI	0.116	Ar XIII	0.120
Si X	0.206	S XII	0.087	Ar XIV	0.087
Si XI	0.167	S XIII	0.075	Ar XV	0.057
Si XII	0.030	S XIV	0.037	Ar XVI	0.012

Note: $\Delta\lambda = \lambda_{\mathrm{HULLAC}} - \lambda_{\mathrm{EBIT}}$ in Å.

and many of the weaker lines as well. But the number and density (here referring to the "crowding" or number of lines per angstrom) of weaker lines can exceed the uncertainty of the calculations and make precise line identification difficult or impossible. Figure 4 shows a comparison of EBIT measurements with HULLAC calculations for Si V – Si VII. While most features are readily identifiable, there are noticeable differences in line strengths and positions, especially in the seemingly straightforward case of the closed-shell neon-like Si V, which on average deviate by over 0.5 Å from calculations. We illustrate the case of silicon here because it showed the most extreme differences between theory and experiment for the elements we published, but large deviations also occurred in sulfur and argon. Accuracy increases as the number of bound electrons decreases and as Z increases, so that in the case of lithium-like Ar XVI, the mean deviation is just a few mÅ (Table 2) [27]. By providing such feedback, laboratory measurements can help theorists further improve the atomic codes.

A new ultra high-resolution (∼4000 at 50 Å) grating spectrometer now gives us the ability to zoom in on complicated regions and resolve finer groupings of lines, albeit with the tradeoff of a narrower wavelength range. Figure 5 shows a comparison of argon taken with the broadband high-resolution and the narrowband ultra high-resolution grating spectrometers on EBIT-I [31].

4. Comparison of laboratory and satellite spectra

Because the spectra from EBIT are taken at a density similar to that of various astrophysical sources, it is possible to compare the spectra for line identification and diagnostics. In Fig. 6, we show a spectrum of the nearby star Procyon (Alpha Canis Minoris) taken with Chandra, overlaid with a spectrum of sulfur taken on EBIT-I. Although the Chandra spectrum has a higher resolution than the EBIT spectrum, sulfur lines are visible — as well as many more lines from other elements. In Fig. 7, we attempt to use the density sensitive line of neon-like Si VII commonly known as M2 (transition $(2p^5_{3/2}3s_{1/2})_{J=2} \rightarrow (2p^6)_{J=0}$), along with the 3F (transition $(2p^5_{1/2}3s_{1/2})_{J=1} \rightarrow (2p^6)_{J=0}$), and also the 3G (transition $(2p^5_{3/2}3s_{1/2})_{J=1} \rightarrow (2p^6)_{J=0}$) lines to determine the density of Procyon's corona. Note that the M2 line is considerably larger

Fig. 9. Sensitivity of magnetic line diagnostic $\mathcal{B}$ for different ions. $\mathcal{B}_{\mathrm{max}}$ is the predicted maximum intensity of line $\mathcal{B}$.

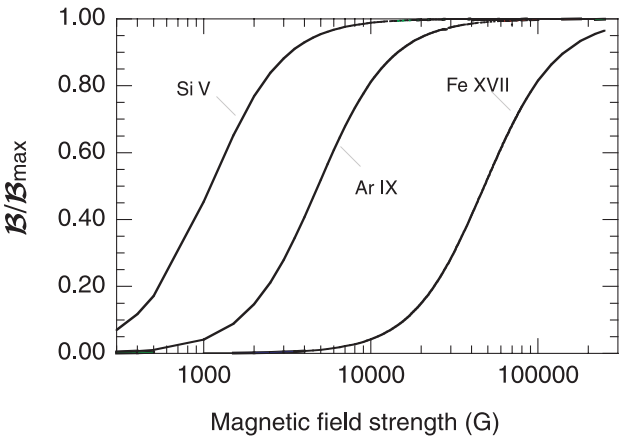

in Procyon (shaded, with a broken line to emphasize the M2 line) than in EBIT (continuous line), indicative of a lower electron density in the former. The ratio curve for the M2/3F and M2/3G lines was calculated with the flexible atomic code [30], and we performed line fittings to the Chandra spectrum to derive the ratio from Procyon. The sulfur M2/3G ratio in Procyon resulted in a derived log density of 10.50 (Fig. 7), but the M2/3F ratio was out of bounds (i.e., did not intersect the ratio curve), perhaps because of blending. In a similar analysis using argon emission lines, the M2/3G ratio resulted in a derived log density of 11.40, while the M2/3F ratio resulted in a derived log density of 11.34. These two densities are very similar to each other but higher than most previous studies.

For example, using various Fe lines observed with EUVE, Schmitt et al. [33] found the average log density to be 9–10, and Pinfield et al. [34] calculated 9.4 using EUVE lines of Fe XI. Similar results were found by Ness et al. [35], who found log densities around 9–9.5 using the Chandra data for helium-like triplets of C, N, and O, while Liang et al. [36] derived log densities of 8.5–9 using Si X. The higher densities we found may be due to Ar IX and S VII being found in a denser portion of Procyon's corona, or they may be due to blending with these weak lines. It may also be possible that the theoretical density curves need to be corrected, as suggested by the results in Sect. 6 below.

5. Discovery of magnetic field diagnostic lines

An unexpected bonus of the work on the EUV line catalogue was the discovery of a class of lines that are sensitive to the strength of the ambient magnetic field [37]. Because these lines increase in strength with the magnetic field, while their neighboring lines do not, the ratios of these lines serve as a diagnostic for magnetic field strength for the extreme ultraviolet and soft X-ray region. Although Zeeman splitting is long known for optical lines, because of line broadening there were no direct techniques available to measure magnetic field strength in the EUV and soft X-ray range.

The new magnetic field diagnostic comes from the $2p^5 3s\,^3\mathrm{P}_0$ level in neon-like systems and mixes with the $2p^5 3s\,^1\mathrm{P}_1$ and the $2p^5 3s\,^3\mathrm{P}_1$ levels in the presence of a magnetic field. There is

Fig. 10. Spectral emission of argon and various indigenous elements from NSTX.

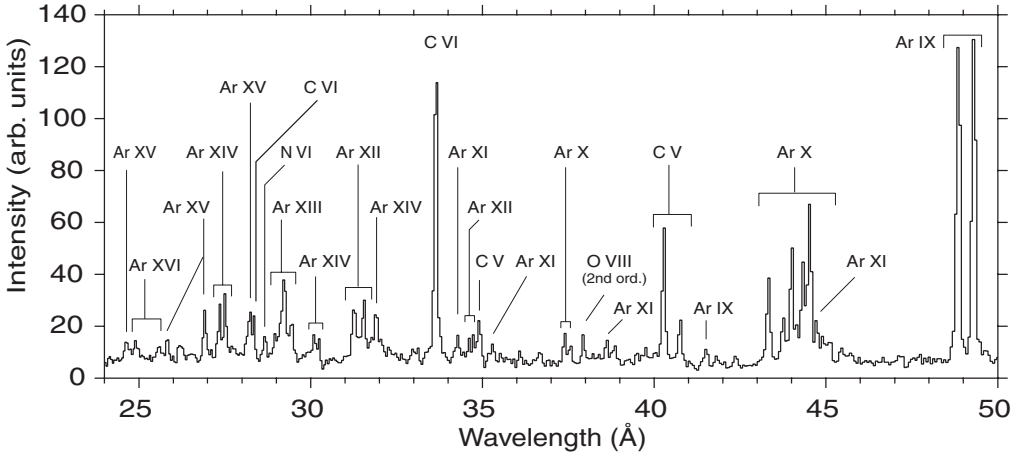

Fig. 11. Comparison of density-sensititve lines in (left) Ar XIV and (right) Ar IX in (top) low-density EBIT plasma and (bottom) high-density NSTX plasma.

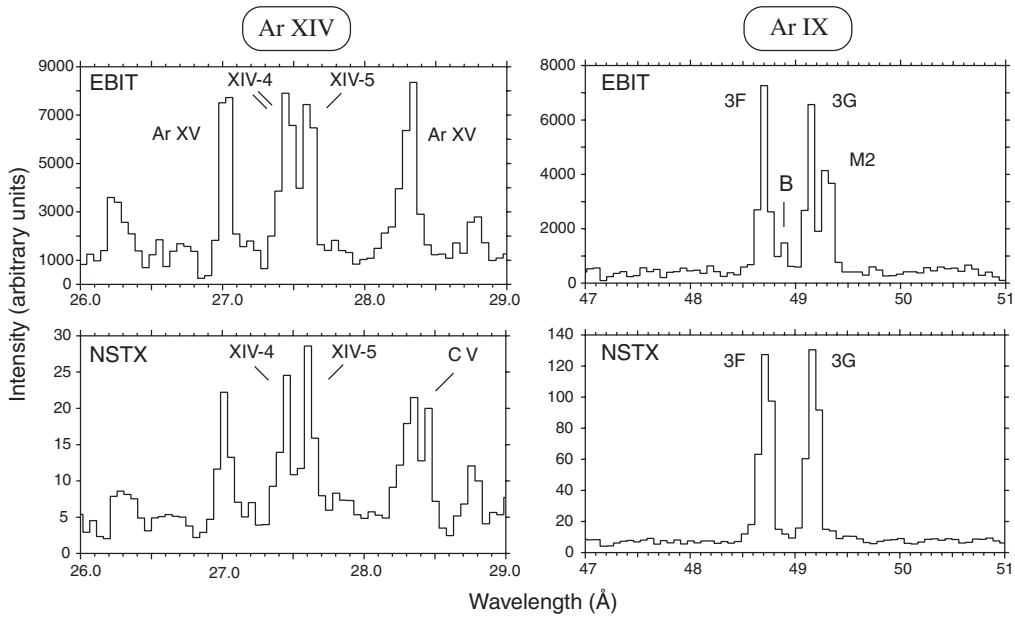

competition between M1 decay to the $2p^5 3s\,^3P_1$ level and X-ray decay to the $J = 0$ ground level, as well as collisional deexcitation at higher densities. Although the $J = 0 \rightarrow J = 0$ transition is strictly forbidden, the line can occur given mixing with the two $J = 1$ levels in a sufficiently strong magnetic field at sufficiently low density. Figure 8 shows the magnetic line in a spectrum of Ar IX. Not only does the line itself vary with magnetic field strength, but ions of different elements become sensitive over a wide range of magnetic field strengths from a few hundred to over 100 000 G (1 G = 0.1 mT) (Fig. 9). Given a wide range in stellar temperatures and magnetic field strengths, this diagnostic feature may be useful in X-ray astrophysics.

6. Calibration of density-sensitive line ratio diagnostics

As described by Graf et al. [38], we recently moved one of the high-resolution variable-spacing (average 2400 lines/mm) grating spectrometers from LLNL to Princeton Plasma Physics Laboratory's NSTX tokamak, where it was dubbed XEUS (X-ray and extreme ultraviolet spectrometer). Because the plasma in NSTX is approximately 100 times as dense as that of EBIT (electron density $\sim 10^{13}$ cm^{-3} versus $\sim 10^{11}$ cm^{-3}) [38], this provides an opportunity to test density-sensitive diagnostic lines over a wide range of astrophysically relevant densities.

We examined density-sensitive lines of Ar IX and Ar XIV in the two machines. Figure. 10 is a spectrum from NSTX showing lines from Ar IX through Ar XVI as well as some of the lines of carbon and oxygen, which are indigenous to NSTX, while Fig. 11 compares spectra from EBIT-I and NSTX. In the case of the $3s \rightarrow 2p$ transitions of Ar IX, the line labelled M2 is prominent in EBIT, but has essentially disappeared in NSTX. In addition, the magnetic line B has also disappeared, reflecting both NSTX's higher density and weaker magnetic field (0.6 T compared to 3 T in EBIT-I). In the case of the $3d \rightarrow 2p$ transitions of Ar XIV, the relative strengths of the lines labelled XIV-4 (tran-

Fig. 12. Comparison of measured and calculated ratios for the density-sensitive Ar XIV lines. Curved lines are calculations for the ratio XIV-5 / XIV-4 (labelled in Fig. 11) from the flexible atomic code, with separate curves for the two different machines. The electron density on EBIT was calculated using the line ratios of the helium-like N VI lines "y" and "z" [39]. Electron density on NSTX was measured directly with multipoint Thomson scattering.

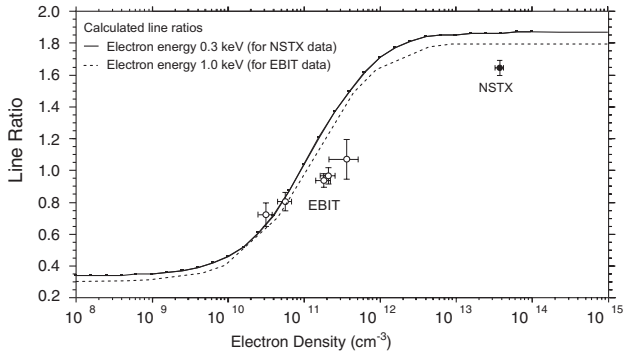

sition $(3d_{3/2})_{3/2} \rightarrow (2p_{1/2})_{1/2}$) and XIV-5 (a blend of transitions $(3d_{5/2})_{5/2} \rightarrow (2p_{3/2})_{3/2}$ and $(3d_{3/2})_{3/2} \rightarrow (2p_{3/2})_{3/2}$) (notation from [8]) have reversed. The density dependence of this line pair was extensively examined on EBIT by Chen et al. [39], who also compared their laboratory measurements with theoretical calculations from the flexible atomic code [30]. A comparison of measured line ratios of XIV-5 over XIV-4, with ratio curves from FAC, is shown in Fig. 12. Note that separate curves were calculated for EBIT (monoenergetic electron beam) and for NSTX (Maxwellian electron distribution), each with its own range. The close similarity of the curves indicates that dependence of the density curves on temperature is essentially negligible. The electron beam density on EBIT varied with beam current, and ratios begin to deviate from predicted at densities above 10^{11}. It was therefore of particular interest to measure this ratio on NSTX, where it is predicted to be at its high-density limit. The measured ratio on NSTX was considerably lower than predicted (Fig. 12), and taken together with the EBIT measurements the laboratory data indicate a rather severe disagreement between theory and experiment. The data clearly suggest an alternative ratio curve.

7. Summary

Electron beam ion traps are very well suited for laboratory astrophysics because they produce plasmas with ionization conditions, electron densities, and line emission similar to those of collisionally excited astrophysical plasmas. The Lawrence Livermore National Laboratory's EBIT facility has been extremely productive in laboratory astrophysics because of its large suite of dedicated spectroscopic instrumentation that has been optimized for such studies. We have produced comprehensive spectral catalogues of a number of astrophysically relevant elements in the soft X-ray and extreme ultraviolet regimes and are continuing analyses of further elements. These catalogues are useful for improving atomic modeling codes and for the analysis of spectra taken by space-based X-ray observatories, such as those of stellar coronae. Studies involving solar and cometary X-rays are detailed elsewhere in this issue [41–43]. The discovery of a new magnetic field X-ray diagnostic emission line in neon-like systems was also made at this facility. Finally, by using the same instruments on the NSTX tokamak, we are able to examine density effects in an extended density range relevant to astrophysical plasmas.

Acknowledgments

This work was supported by NASA's Astronomy and Physics Research program under Contract no. NNH04AA751 and was performed under the auspices of the Department of Energy by the University of California Lawrence Livermore National Laboratory under Contract No. W-7405-ENG-48. The authors thank two anonymous reviewers for their comments and criticisms, which greatly improved this paper.

References

1. H. Friedman, S.W. Lichtman, and E.T. Byram. Phys. Rev. **83**, 1025 (1951).
2. R. Giacconi, H. Gursky, and F.R. Paolini. Phys. Rev. Lett. **9**, 439 (1962).
3. F.B.S. Paerels and S.M. Kahn. Annu. Rev. Astron. Astroph. **41**, 291 (2003)
4. P. Beiersdorfer. Electron-ion interaction cross-sections determined by X-ray spectroscopy on EBIT. *In* Electron and Atomic Collisions - XVII, ICPEAC. Brisbane, 1991. *Edited by* W.R. MacGillivray, I.E. McCarthy, and M.C. Standage. Hilgar, Bristol, UK. 1992. pp. 313–322.
5. S.M. Kahn, P. Beiersdorfer, G.V. Brown, V. Decaux, M.F. Gu, D.A. Liedahl, D.W. Savin, S.B. Utter, and K. Widmann. Laboratory X-ray spectroscopy in experiments in support of NASA's X-ray satellite missions. *In* Proc. Lab. Space Sci. Workshop. Cambridge, Mass. 1–3 April 1998.
6. P. Beiersdorfer. Annu. Rev. Astron. Astroph. **41**, 343 (2003).
7. P. Beiersdorfer. *In* X-ray and inner-shell processes. AIP Conf. Procs, No. 215, Knoxville, Tenn. 1990. *Edited by* T.A. Carlson, M.O. Krause, and S.T. Manson. AIP, N.Y. 1990. p. 648.
8. J.K. Lepson, P. Beiersdorfer, E. Behar, and S.M. Kahn. Astrophys. J. **590**, 604 (2003).
9. G.A. Doschek. *In* Extreme ultraviolet astronomy. *Edited by* R.T. Malina and S. Bowyer. Pergamon, N.Y. 1991.
10. A.K. Dupree and S.J. Kenyon. *In* Extreme ultraviolet astronomy. *Edited by* R.T. Malina and S. Bowyer. Pergamon, N.Y. 1991.
11. R. Mewe. Astron. Astrophys. Rev. **3**, 127 (1991).
12. H.E. Mason and B.C. Monsignori Fossi. Astron. Astrophys. **6**, 123 (1994).
13. N.S. Brickhouse, J.C. Raymond, and B.W. Smith. Astrophys. J. **S97**, 551 (1995).
14. K.P. Dere, E. Landi, H.E. Mason, B. Monsignori Fossi, and P.R. Young. Astron. Astrophys. Suppl. **125**, 149 (1997).
15. K.P. Dere, E. Landi, P.R. Young, and G. Del Zanna. Astrophys. J. **134**, S331 (2001).
16. On-line data base available at http://www.arcetri.astro.it/science/chianti/chianti.html
17. R. Mewe, J.S. Kaastra, and D.A. Liedahl. Legacy, **6**, 16 (1995).
18. R. Mewe, J.S. Kaastra, C.J. Schrijver, G.H.J. van den Oord, and F.J.M. Alkemade. Astron. Astrophys. Suppl. **296**, 477 (1995).
19. P. Beiersdorfer, J.K. Lepson, G.V. Brown, S.B. Utter, S.M. Kahn, D.A. Liedahl, and C.W. Mauche. Astrophys. J. **519**, L185 (1999).

20. G.V. Brown, P. Beiersdorfer, D.A. Liedahl, K. Widmann, and S.M. Kahn. Astrophys. J. **502**, 1015 (1998).
21. J.K. Lepson, P. Beiersdorfer, G.V. Brown, D.A. Liedahl, S.B. Utter, N.S. Brickhouse, A.K. Dupree, J.S. Kaastra, R. Mewe, and S.M. Kahn. Astrophys. J. **578**, 648 (2002).
22. G.V. Brown, P. Beiersdorfer, D.A. Liedahl, K. Widmann, S.M. Kahn, and E.J. Clothiaux. Astrophys. J. Suppl. **140**, 589 (2002).
23. H. Chen, M.F. Gu, E. Behar, G.V. Brown, S.M. Kahn, and P. Beiersdorfer. Astrophys. J. **S168**, 319 (2007).
24. M.F. Gu, P. Beiersdorfer, G.V. Brown, H. Chen, D.B. Thorn, and S.M. Kahn. Astrophys. J. **657**, 1172 (2007).
25. M.-F. Gu. Astrophys. J. **156**, S105 (2005).
26. J.K. Lepson, P. Beiersdorfer, E. Behar, and S.M. Kahn. Astrophys. J. **625**, 1045 (2005).
27. J.K. Lepson, P. Beiersdorfer, E. Behar, and S.M. Kahn. Nucl. Instrum. Methods Phys. Res. Sect. B, **235**, 131 (2005).
28. A. Bar-Shalom, M. Klapisch, and J. Oreg. J. Quant. Spectrosc. Radiat. Transfer, **71**, 169 (2001).
29. R. Doron and E. Behar. Astrophys. J. **574**, 518 (2002).
30. M.-F. Gu. Astrophys. J. **582**, 1241 (2003).
31. P. Beiersdorfer, E. Magee, E. Träbert, H. Chen, J.K. Lepson, M.F. Gu, and M. Schmidt. Rev. Sci. Instrum. **75**, 3723 (2004).
32. A.J.J. Raassen, R. Mewe, M. Audard, M. Güdel, J.S. Kaastra, R.L.J. van der Meer, C.R. Foley, and J.-U. Ness. Astron. Astrophys. **389**, 228 (2002).
33. J.H.M.M. Schmitt, J.J. Drake, B.M. Haisch, and R.A. Stern. Astrophys. J. **467**, 841 (1996).
34. D.J. Pinfield, F.P. Keenan, M. Mathioudakis, K.G. Widing, P.T. Gallagher, G.P. Gupta, S.S. Tayal, R.J. Thomas, and J.W. Brosius. Astrophys. J. **562**, 566 (2001).
35. J.-U. Ness, R. Mewe, J.H.M.M. Schmitt, A.J.J. Raassen, D. Porquet, J.S. Kaastra, R.L.J. van der Meer, V. Burwitz, and P. Predehl. Astron. Astrophys. **367**, 282 (2001).
36. G.Y. Liang, G. Zhao, and J.R. Shi. Astron. J. **132**, 371 (2006).
37. P. Beiersdorfer, J.H. Scofield, and A.L. Osterheld. Phys. Rev. Lett. **90**, 235003 (2003).
38. A.T. Graf, S. Brockington, R. Horton, S. Howard, D. Hwang, P. Beiersdorfer, J. Clementson, D. Hill, M. May, H. McClean, R. Wood, M. Bitter, J. Terry, W.L. Rowan, J.K. Lepson, and L. Delgado-Aparicio. Can. J. Phys. **86**, this issue (2008).
39. H. Chen, P. Beiersdorfer, L.A. Heeter, D.A. Liedahl, K.L. Naranjo-Rivera, E. Träbert, M.F. Gu, and J.K. Lepson. Astrophys. J. **611**, 598 (2004).
40. G.V. Brown, P. Beiersdorfer, D.A. Liedahl, K. Widmann, and S.M. Kahn. Astrophys. J. **502**, 1015 (1998).
41. G.V. Brown. Can. J. Phys. **86**, (2008). This issue.
42. B.J. Wargelin, P. Beiersdorfer, and G.V. Brown. Can. J. Phys. **86**, (2008). This issue.
43. S. Otranto, R.E. Olson, and P. Beiersdorfer. Can. J. Phys. **86**, (2008). This issue.